

THE FIRST X-SHOOTER OBSERVATIONS OF JETS FROM YOUNG STARS*

F. BACCIOTTI¹, E. T. WHELAN², J. M. ALCALÁ³, B. NISINI⁴, L. PODIO⁵, S. RANDICH¹, B. STELZER⁶, AND G. CUPANI⁷

¹ INAF-Osservatorio Astrofisico di Arcetri, Largo E. Fermi 5, 50125 Firenze, Italy

² Laboratoire d'Astrophysique de l'Observatoire de Grenoble, UMR 5521 du CNRS, 38041 Grenoble Cedex, France

³ INAF-Osservatorio di Capodimonte, Via Moiariello 16, 80131 Napoli, Italy

⁴ INAF-Osservatorio di Roma, Via di Frascati 33, 00040, Monteporzio Catone, Italy

⁵ Kapteyn Astronomical Institute, Landleven 12, 9747 AD Groningen, The Netherlands

⁶ INAF-Osservatorio di Palermo, Piazza del Parlamento 1, 90134 Palermo, Italy

⁷ INAF-Osservatorio di Trieste, Via Tiepolo 11, 34143 Trieste, Italy

Received 2011 April 20; accepted 2011 June 16; published 2011 July 26

ABSTRACT

We present the first pilot study of jets from young stars conducted with X-shooter, on the ESO/Very Large Telescope. As it offers simultaneous, high-quality spectra in the range 300–2500 nm, X-shooter is uniquely important for spectral diagnostics in jet studies. We chose to probe the accretion/ejection mechanisms at low stellar masses examining two targets with well-resolved continuous jets lying on the plane of the sky: ESO-HA 574 in Chameleon I and Par-Lup3-4 in Lupus III. The mass of the latter is close to the sub-stellar boundary ($M_* = 0.13 M_\odot$). A large number of emission lines probing regions of different excitation are identified, position–velocity diagrams are presented, and mass outflow/accretion rates are estimated. Comparison between the two objects is striking. ESO-HA 574 is a weakly accreting star for which we estimate a mass accretion rate of $\log(\dot{M}_{\text{acc}}) = -10.8 \pm 0.5$ (in $M_\odot \text{ yr}^{-1}$), yet it drives a powerful jet with $\dot{M}_{\text{out}} \sim 1.5\text{--}2.7 \times 10^{-9} M_\odot \text{ yr}^{-1}$. These values can be reconciled with a magneto-centrifugal jet acceleration mechanism assuming that the presence of the edge-on disk severely depresses the luminosity of the accretion tracers. In comparison, Par-Lup3-4, with stronger mass accretion ($\log(\dot{M}_{\text{acc}}) = -9.1 \pm 0.4 M_\odot \text{ yr}^{-1}$), drives a low-excitation jet with about $\dot{M}_{\text{out}} \sim 3.2 \times 10^{-10} M_\odot \text{ yr}^{-1}$ in both lobes. Despite the low stellar mass, $\dot{M}_{\text{out}}/\dot{M}_{\text{acc}}$ for Par-Lup3-4 is at the upper limit of the range usually measured for young objects, but still compatible with a steady magneto-centrifugal wind scenario if all uncertainties are considered.

Key words: ISM: jets and outflows – stars: formation

1. INTRODUCTION

Collimated outflows are common to accreting objects with a wide variety of spatial scales and mass accretion rates, but the phenomenon is best studied in the case of jets from the nearby low-mass stars in their pre-main-sequence phase (Ray et al. 2007; Whelan et al. 2009). These flows present characteristic spectra rich in shock-excited emission lines (Ray et al. 2007; Hartigan et al. 1994) that allow a detailed diagnostic of the kinematic and physical properties of the gas. To better understand the enigmatic process of jet generation, it is imperative to determine the exact relationship between outflows and accretion. Their interplay is at the heart of the widely accepted theory of magneto-centrifugal launching that may be common to all jet-generating objects (Ferreira et al. 2006; Pudritz et al. 2007; Shang et al. 2007). The pertinent models prescribe stringent constraints for the ratio of accreted to ejected mass outflow rates, and it is important to understand how this relationship changes with the mass of the driving sources and in particular for low stellar masses (Whelan et al. 2010).

The spectra of stellar jets can today be efficiently analyzed with dedicated diagnostics of key lines, and estimates of mass outflow rates (\dot{M}_{out}) can be compared with corresponding mass accretion rates (\dot{M}_{acc} ; Bacciotti & Eislöffel 1999; Masciadri & Raga 2004; Podio et al. 2006; Hartigan & Morse 2007). Reliable estimates of $\dot{M}_{\text{out}}/\dot{M}_{\text{acc}}$, however, can only be given if one has detailed knowledge of the excitation properties of the gas in each

location. It is thus critical to have complete spectral mapping along the jet extension in the largest possible wavelength range.

With these ideas in mind we chose to characterize the jets of ESO-HA 574 and Par-Lup3-4, two intriguing objects included in a pilot study of young stars of low and sub-stellar mass with X-shooter. Mounted on the Unit Telescope 2 of the Very Large Telescope, X-shooter is an instrument providing high-quality, medium resolution, UVB (300-559.5 nm), VIS (559.5-1024 nm), and NIR (1024-2480 nm) spectra. This wavelength range includes a large number of emission lines typical of both outflow and accretion phenomena, making X-shooter currently unequaled in spectral diagnostic studies.

The outflows from the selected sources have a continuous jet-like morphology and lie close to the plane of the sky, which makes them well resolved spatially with no superposition of the blue and red lobes, and with minimal obscuration by the disk.

Our first target is ESO-HA 574 ($11^{\text{h}}16^{\text{m}}03^{\text{s}}7, -76^{\circ}24'53''$), a low-luminosity, low-mass source discovered by Comerón et al. (2004) in a study of the Chameleon I star-forming region ($d = 160 \pm 17$ pc; Wichmann et al. 1998). Its bolometric luminosity is only $0.0034 L_\odot$ (Luhman 2007), which, compared with other typical T Tauri stars of the same spectral type (K8) in Chameleon I, makes this star underluminous by a factor of about 150. This is probably caused by the edge-on viewing geometry of its disk. The lines normally used for accretion diagnostics are also very weak (Comerón et al. 2004), which may suggest low levels of accretion, yet the star powers a well-developed bipolar jet (HH 872, of total length of 3150 AU) at a position angle (P.A.) of $\sim 45^\circ$, revealed in follow-up FORS1 [S II] imaging by Comerón & Reipurth (2006). The jet is made up of five distinct

* Based on Observations collected with X-shooter at the Very Large Telescope on Cerro Paranal (Chile), operated by the European Southern Observatory (ESO). Program ID: 085.C-0238(A).

knots, with knots A, B, C, D forming the blueshifted jet, and knot E in the redshifted lobe.

The second target, Par-Lup3-4 ($16^{\text{h}}08^{\text{m}}51^{\text{s}}44, -39^{\circ}05'30''.5$), was first reported by Nakajima et al. (2000) as part of a near-infrared survey of the Lupus III dark cloud ($d = 200 \pm 40$ pc; Comerón et al. 2003). Its mass is only $\sim 0.13 M_{\odot}$, but the accretion tracers in the spectrum are quite strong and indicate a mass accretion rate of $\dot{M}_{\text{acc}} = 1.4 \times 10^{-9} M_{\odot} \text{ yr}^{-1}$ (Comerón et al. 2003). The forbidden lines are associated with a small collimated jet (HH 600) at P.A. $\sim 130^{\circ}$ (Fernández & Comerón 2005; Comerón & Fernández 2011). The source is underluminous by a factor of about 25 with respect to other M5 young stars in Lupus III, its bolometric luminosity being $0.003 L_{\odot}$ (Merín et al. 2008). An edge-on disk oriented at about 81° is probably responsible for the subluminescence (Huélamo et al. 2010).

We extend these studies, which were limited to the visual band, by taking X-shooter spectra of the targets with the slit parallel to the jet axis. Thus in a single observation, and for the first time in the field of stellar jet studies, we obtained a simultaneous, complete spectral mapping from 300 nm to $2.2 \mu\text{m}$ that provided immediate and far-reaching information about the physical properties of the outflows and of their sources. In this Letter, we present the spectra and discuss the accretion/outflow properties of the two targets. A complete mapping of the jet physical conditions derived from the same data sets is the subject of a subsequent paper.

2. OBSERVATIONS AND DATA REDUCTION

The observations were conducted on 2010 April 7 (Program ID: 085.C-0238(A)), as part of the INAF/GTO program on star-forming regions (Alcalá et al. 2011). The seeing varied between $0''.9$ and $1''.2$. In both cases the $11''$ long slit was aligned with the jet axis, along P.A. $44^{\circ}8$ and $130^{\circ}0$ for ESO-HA 574 and Par-Lup3-4, respectively (see above). The total exposure time per star was 3600 s (4×900) in all arms and nodding observing mode “ABBA” was used (shifting along the jet P.A.) in order to minimize the contribution of the background in the near-infrared (NIR). Slit widths of $1''.0$, $0''.9$, and $0''.9$ were used, yielding resolving powers of 5100, 8800, and 5600 (corresponding to about 58, 34, and 53 km s^{-1} velocity resolution) for the UVB, VIS, and NIR arms, respectively. The data reduction was performed independently for each arm using the X-shooter pipeline version 1.1.0 (Modigliani et al. 2010). One-dimensional spectra were then extracted over the star continuum and over the extension of the knots. Note that the latter appear only in either the A or B nodding position, so the spectra over each knot correspond to an integration time of 1800 s. The reported radial velocities are systemic, with the LSR velocity of the sources determined using the photospheric absorption line of KI $\lambda 7698$ (VIS arm). For ESO-HA 574 we measured $v_{\text{LSR}} = +3 \text{ km s}^{-1}$, while for Par-Lup 3-4 $v_{\text{LSR}} = 5.5 \text{ km s}^{-1}$, in agreement with the LSR velocities of the corresponding clouds, measured from CO observations to be 4 and $7 \pm 2 \text{ km s}^{-1}$, respectively (Dame et al. 1987). On-source spectra were extinction corrected assuming for ESO-HA 574 $A_v = 1.7$ mag (derived from $A_J = 0.45$ (Luhman 2007), using the extinction curve at $R_v = 3.1$ from Savage & Mathis 1979) and $A_v = 3.5$ mag for Par-Lup3-4 (Huélamo et al. 2010; Comerón et al. 2004). Nevertheless, for both targets, A_v values around zero are derived off-source using the [Fe II] lines at $1.27, 1.32, 1.64 \mu\text{m}$ that trace the jet emission (Nisini et al. 2005). This suggests that the jet propagates out

of the envelope obscuring the star, and therefore the spectra extracted for the jet knots were not dereddened.

3. RESULTS

Figure 1 shows the X-shooter spectrum of ESO-HA 574 extracted at the source position, obtained by summing over 5 to 7 pixel rows ($0''.9$ to $1''.1$, depending on the point-spread function of the considered arm). The system is observed in numerous lines, including both accretion and ejection tracers. Balmer lines from H9 to H α are identified, as well as the calcium triplet and He I at $1.083 \mu\text{m}$ and Pa β , while Br γ is not detected. Among the many forbidden lines, we find strong lines of sulfur, oxygen, nitrogen, and iron in multiple ionization states. As noted by Comerón et al. (2004), the forbidden [Ca II] $\lambda 7321, 7324$ lines are much more prominent than the calcium triplet, supporting the idea that both the stellar continuum and the accretion tracers are occulted by the edge-on disk, while the jet tracers are unaffected (as it occurs in the edge-on system T Cha studied by Schisano et al. 2009).

In Figure 2, we present position–velocity (PV) diagrams of a selection of key lines. Knots A and B (jet) and knot E (counterjet) are indicated in the [S II] $\lambda 6731$ panel. Knot A1, identified in Comerón & Reipurth (2006) as the source, has actually moved to about $0''.2$ with respect to the star continuum. The emission in H α and H β as well as in [O II] $\lambda\lambda 3726, 3729$ and [S II] $\lambda 6731$ lines is extended, with higher dispersion close to the star and in knot E which has a bow-shock shape. On the contrary, the emission in the H $_2$ lines is concentrated around the star, as is often the case in Classical T Tauri stars (CTTSs), likely originating in shocked walls of a cavity opened by the flows (Beck et al. 2008). In general the lines present low systemic radial velocities, with knots A and B blueshifted at ~ -3 and $\sim -6 \text{ km s}^{-1}$ in [S II] $\lambda 6731$, while knot E is redshifted at $+25 \text{ km s}^{-1}$. Tangential velocities were determined by comparison with the [S II] images of Comerón & Reipurth (2006), taken on 2005 July 21. We find $V_{\text{tan}} = 130, 220, \text{ and } 325 \text{ km s}^{-1}$ for knots A, B, and E, respectively. Large knot velocity differences and velocity asymmetries in opposed jet lobes are commonly observed in CTTS jets (Hirth et al. 1994; Podio et al. 2011). The determined velocities suggest very low jet inclination angles of only $1^{\circ}3$, $1^{\circ}6$, and 4° at knots A, B, and E, respectively, confirming that the disk is nearly edge-on, and it is causing the observed underluminosity (Comerón et al. 2004).

Turning to Par-Lup3-4, the full spectrum on-source (integrated over the $1''$ of the continuum width) is shown in Figure 3 and three selected PV diagrams in Figure 2 (bottom). Far fewer jet tracers are detected than in ESO-HA 574, while accretion signatures like the calcium triplet at 8500 \AA are stronger. Both Pa β and Br γ are present here. Only a few lines are extended, notably the [S II] lines, which show a well-developed bipolar structure, extending to $\sim 2''.5$ (500 AU) on both sides. Radial velocities up to -20 and $+20 \text{ km s}^{-1}$ are measured, consistently with the LSR velocities of -18.3 and $+23.6 \text{ km s}^{-1}$ determined by Fernández & Comerón (2005) in the same line. The strong [O I] $\lambda 6300$ line is also extended, although the redshifted component is affected by subtraction of the [O I] atmospheric emission (see the inset in Figure 2). The weak [N II] $\lambda 6583$ also shows traces of bipolarity, over similar radial velocities. Tangential velocities have been reported recently by Comerón & Fernández (2011) to be $170 \pm 30 \text{ km s}^{-1}$ in both jet lobes, which, combined with our radial velocities, give a jet inclination angle of about 7° .

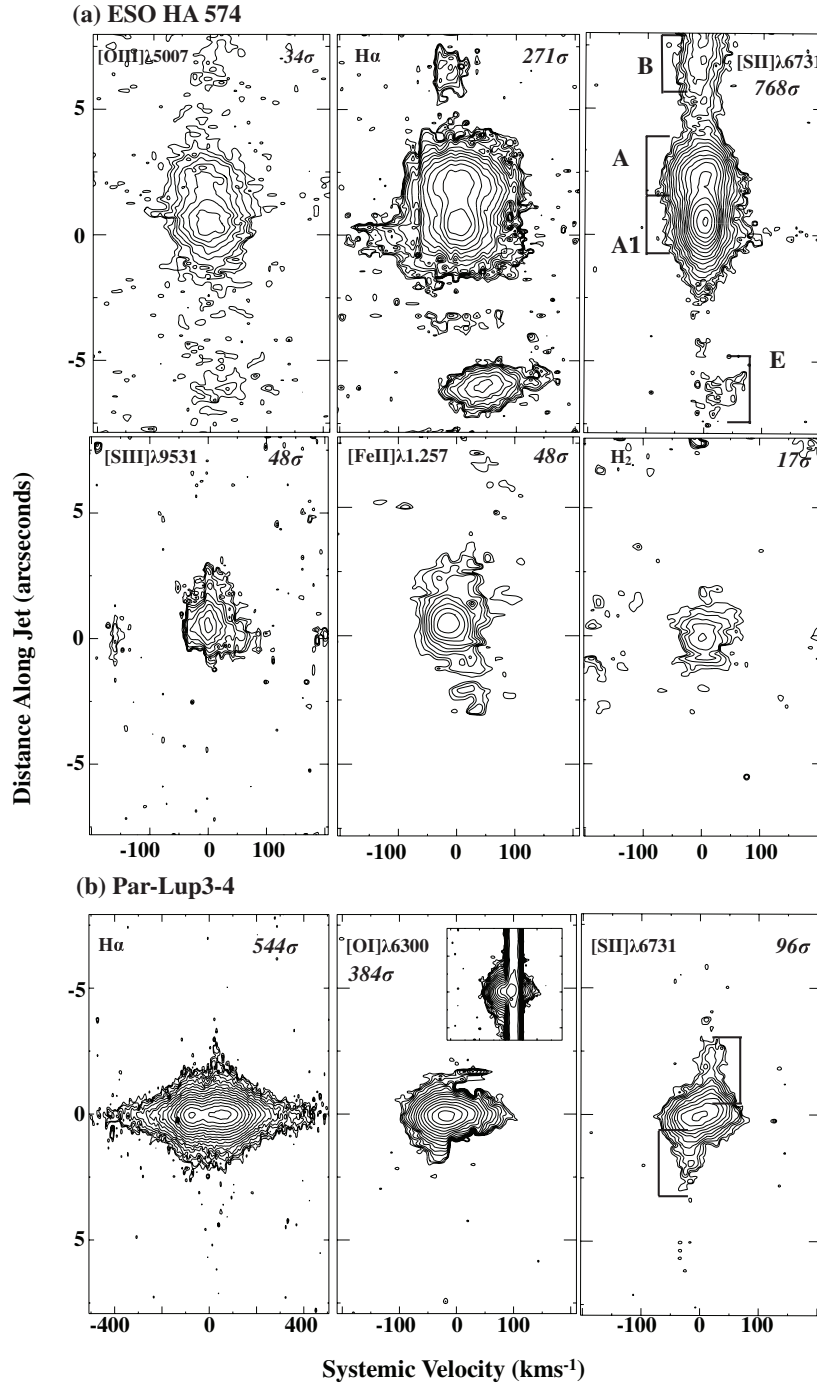


Figure 2. PV diagrams of selected lines around ESO-HA 574 and Par-Lup 3-4. Contours begin at three times the rms noise and increase by a factor of $\sqrt{2}$. The peak value is shown in the upper right corners. One-dimensional spectra of the knots in the ESO-HA 574 jet and the two lobes of the Par-Lup3-4 jets were extracted over the regions marked on the [S II] λ 6731 panels. Distances along the blueshifted lobe have positive y values.

the obscuration caused by the edge-on disk. Indeed, assuming that both the continuum and the accretion tracers are depressed by the same amount, the correction for the disk occultation on L_* , and, consequently, on R_* and L_{acc} , would result in a mass accretion rate of $\sim 1.7 \times 10^{-8} M_{\odot} \text{ yr}^{-1}$, in line with other stars of similar mass (Natta et al. 2004). On the contrary, for Par-Lup3-4 M_{acc} is just above the typical value for similar stars, suggesting that the 81° inclination of the disk plane (Huélamo et al. 2010) leaves the accretion funnels visible at least in part.

A comparison of the $H\alpha$ profile in the two targets is given in the bottom panels of Figure 4. For ESO-HA 574 the ma-

jority of the $H\alpha$ emission is extended and relatively narrow ($-100, +100 \text{ km s}^{-1}$), superimposed on a much weaker broad component ($-300, +300 \text{ km s}^{-1}$), localized at the star continuum. On the contrary, in Par-Lup3-4 the $H\alpha$ line is concentrated around the star, it is broad (10% width $\sim 350 \text{ km s}^{-1}$), and its shape is normally not associated to a jet component (type II B profile in the classification of Reipurth et al. 1996). In order to disentangle the emission pertinent to accretion or ejection, the $H\alpha$ line profiles were analyzed with spectro-astrometry, a technique that allows one to find positional displacements of the line peak with respect to the

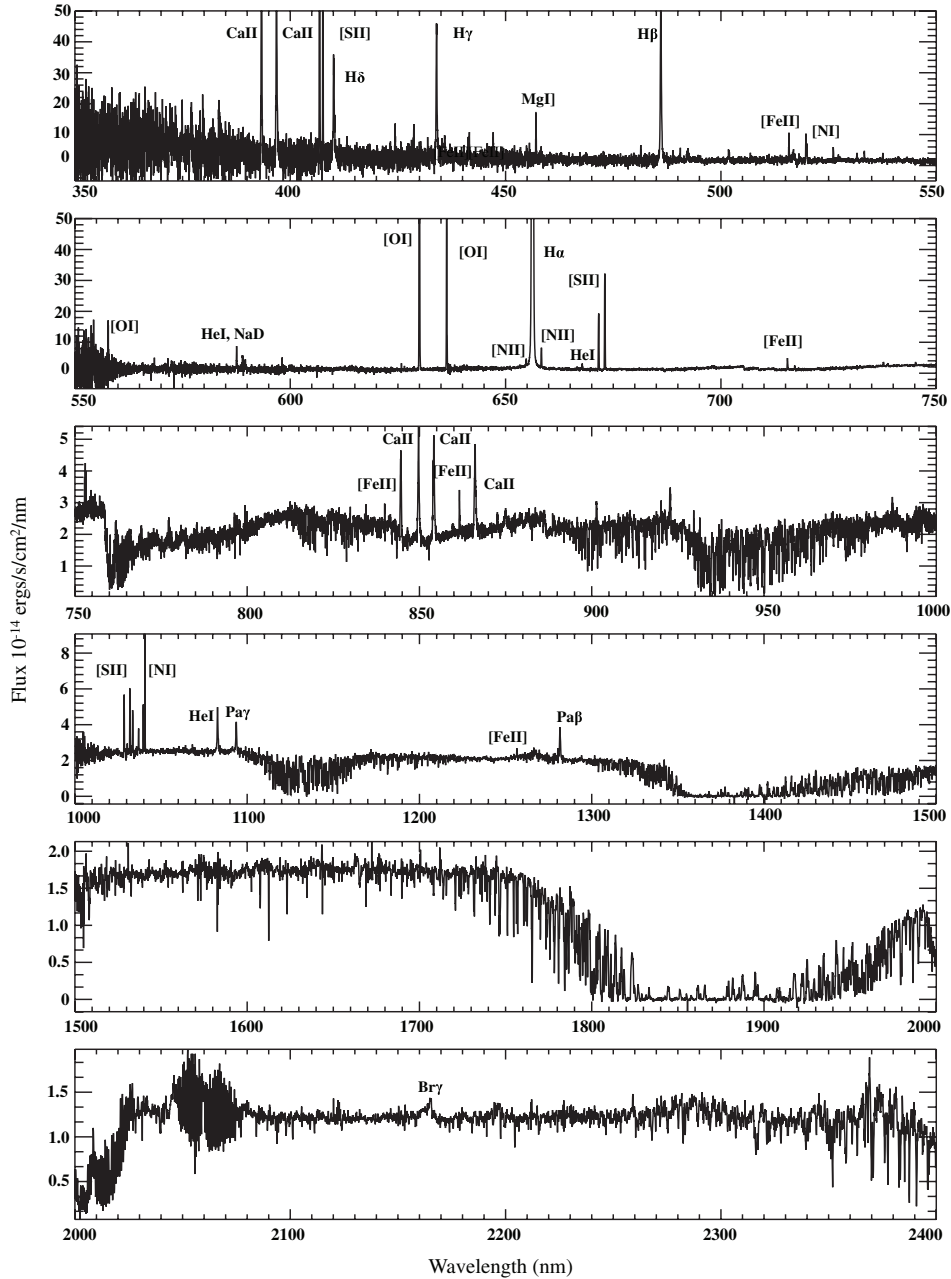


Figure 3. Same as Figure 1, for Par-Lup3-4. The spectrum is extinction-corrected for $A_v = 3.5$.

star continuum over angular distances of a few tens of milliarcseconds (for details see Whelan & Garcia 2008). The absence of any significant offset for Par-Lup 3-4 is consistent with the disappearance of the jet in $H\alpha$ in the 2010 images of Comerón & Fernández (2011) and suggests an accretion origin for this line. The same applies for the broad $H\alpha$ component in ESO-HA 574, while the jet portion between $\pm 100 \text{ km s}^{-1}$ obviously has a large offset, preventing the use of accretion diagnostics based on the width at 10% intensity (Natta et al. 2004).

Regarding the jets, X-shooter fully reveals its power, showing at once the actual excitation state of the gas along the flow. Figure 2 shows that in ESO-HA 574 strong $[\text{O III}]\lambda 5007$ and $[\text{S III}]\lambda 9531$ lines are observed. The knots closer to the source (A1, A) present the highest excitation and density as also probed by $[\text{S II}]\lambda 4069$, $[\text{N II}]\lambda 6583$, and by the $[\text{S II}]$ and $[\text{N I}]$ lines at

$1.03/1.04 \mu\text{m}$. The emission in the helium line at $1.083 \mu\text{m}$ is also very strong, and spatially extended, as has been found in other CTTs (Takami et al. 2002; Podio et al. 2008). This line is a probe of inner wind regions (Kwan et al. 2007), and indicates high electron temperatures ($T_e \sim 10^4 \text{ K}$) and densities ($n_e > 10^6 \text{ cm}^{-3}$). In the same way, in Par-Lup3-4 the absence of lines from high ionization states and the strength of $[\text{O I}]$ and $[\text{N I}]$ lines with respect to $[\text{N II}]$ lines reveal that the gas in this jet has a low excitation state along the flow.

Importantly, this qualitative inspection indicates that the usual diagnostic procedures to estimate mass outflow rates (Bacciotti & Eisloffel 1999; Podio et al. 2006) cannot be applied for ESO-HA 574, as the abundances of the species considered (O I , Fe II , N I) should be calculated considering high ionization levels. On the other hand, in the Par-Lup 3-4 jet, intrinsically of low-excitation, $[\text{N II}]$ lines are extremely faint and $[\text{O I}]$ lines

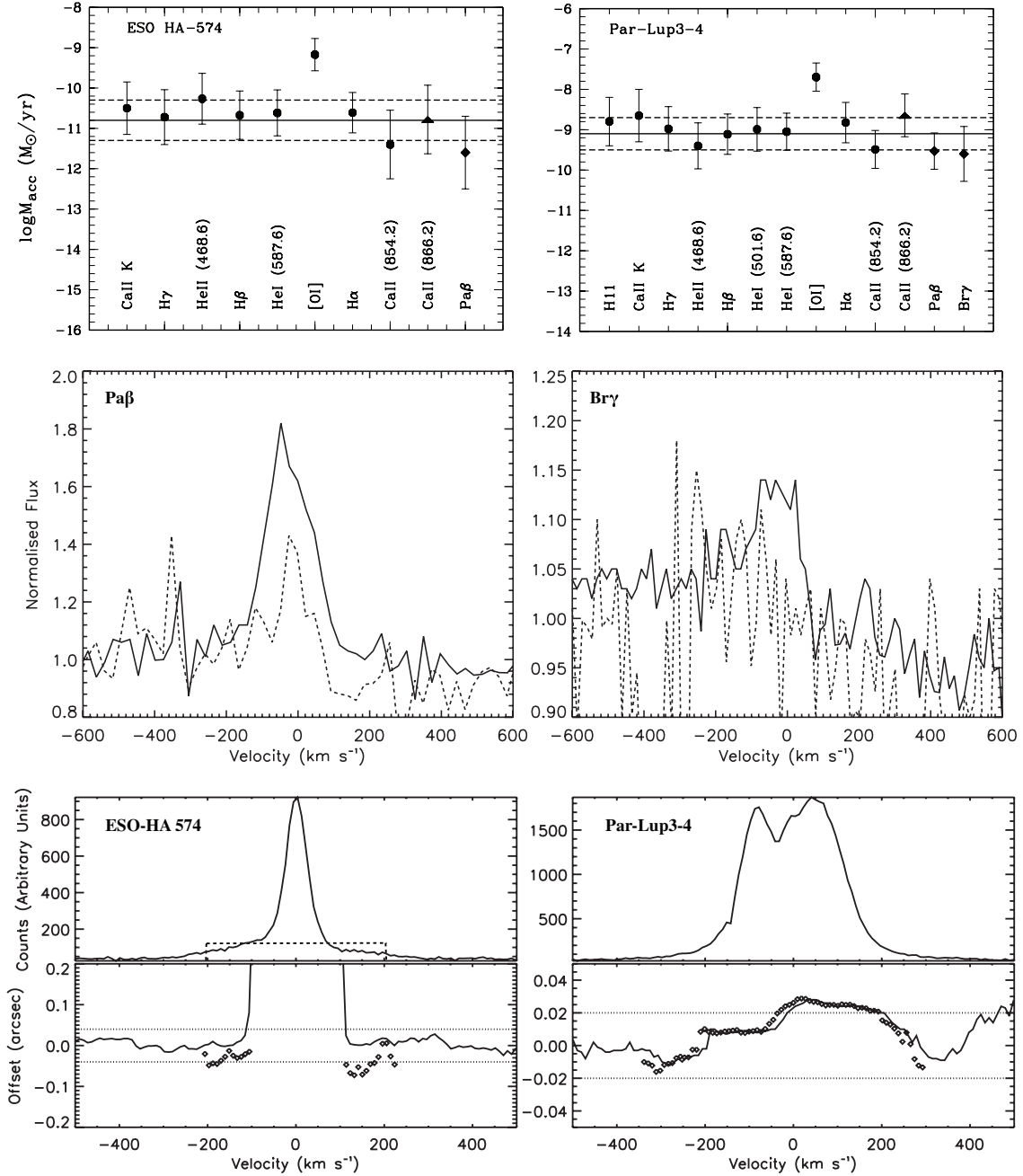


Figure 4. Top: mass accretion rates from different accretion tracers. Solid line: average (excluding [O I]); dashed line: $\pm 1\sigma$ standard deviation. Middle: Pa β and Br γ in ESO-HA 574 (dashed line) and Par-Lup3-4 (solid line), normalized to their continua. Bottom: spectro-astrometric signal in H α , before (solid curve) and after (diamonds) continuum subtraction. Positive offsets are along the blueshifted jet (dashed lines: spectro-astrometric accuracy).

are contaminated by the sky lines. Therefore, here we give only a preliminary estimate of the mass outflow rates (\dot{M}_{out}) from the [S II] λ 6731 line luminosity in the knots where [S III] lines are not detected. Following the method in Hartigan et al. (1995), in each knot \dot{M}_{out} is calculated as

$$\dot{M}_{\text{out}}(M_{\odot} \text{ yr}^{-1}) = 4.51 \times 10^9 \left(1 + \frac{n_c}{n_e} \right) \times L_{[\text{S II}]\lambda 6731}(L_{\odot}) \frac{V_{\text{tan}}(\text{km s}^{-1})}{l_{\text{tan}}(\text{cm})}, \quad (1)$$

where n_c is the critical density for the [S II] ratio ($2 \times 10^4 \text{ cm}^{-3}$), while V_{tan} and l_{tan} are the tangential velocity and the knot length,

respectively. The line ratios and luminosities were estimated from one-dimensional spectra extracted over the spatial regions marked in Figure 2 ([S II] λ 6731 panel), with no correction for extinction (see Section 2). The errors are propagated from the noise level around the [S II] lines and from the distance to the star.

The results are collected in Table 1. For ESO-HA 574, n_e turns out to be 1750, 280, and 110 cm^{-3} for knots A, B, and E, respectively, well below the critical density. In knot A1 $n_e = 3000 \pm 130 \text{ cm}^{-3}$, but \dot{M}_{out} could not be estimated because [S III] lines are detected here, while the method assumes sulfur to be all singly ionized. In the other knots, \dot{M}_{out} turns out to be $(1.5\text{--}3) \times 10^{-9} M_{\odot} \text{ yr}^{-1}$, within the usual range found for CTTS jets (Hartigan et al. 1995; Melnikov et al. 2009).

Table 1
Mass Outflow Rates in Jets from ESO-HA 574 and Par-Lup3-4, Estimated from the Luminosity of the [S II] λ 6731 Line

Object	n_e (10^3 cm^{-3})	$L_{[\text{S II}]\lambda 6731}$ ($10^{-7} L_{\odot}$)	V_{tan} (km s^{-1})	l_{tan} (10^{15} cm)	\dot{M}_{out} ($M_{\odot} \text{ yr}^{-1}$)
ESO HA 574					
Knot A	1.7 ± 0.1	7.7 ± 0.5	130 ± 30	3.8 ± 0.4	$1.5 \pm 0.4 \times 10^{-9}$
Knot B	0.28 ± 0.03	2.4 ± 0.4	220 ± 50	6.5 ± 0.7	$2.7 \pm 1 \times 10^{-9}$
Knot E	0.11 ± 0.1	0.42 ± 0.07	325 ± 50	5.3 ± 0.6	$2.5 \pm 2 \times 10^{-9}$
Par-Lup3-4					
Blue lobe	1150 ± 20	1.85 ± 0.3	170 ± 30	7.2 ± 1.5	$3.6 \pm 0.6 \times 10^{-10}$
Red lobe	3200 ± 50	5.2 ± 0.5	170 ± 30	9.0 ± 1.8	$3.2 \pm 0.3 \times 10^{-10}$

Notably, values are similar along the flow, as expected if no big sideways losses are present (due, e.g., to large bow-shocks), and, as in other asymmetric jets, they are about the same in the two lobes, despite the gas having different physical conditions (see Podio et al. 2011 for a discussion). The obtained \dot{M}_{out} , however, appears two orders of magnitude higher than the derived \dot{M}_{acc} , if the latter is taken at face value. As discussed above, however, the occultation of the edge-on disk should be taken into account. A correction of \dot{M}_{acc} for the observed underluminosity would bring the mass ejection/accretion ratio back to ≈ 0.3 (over the two lobes), in the expected range for magneto-centrifugal jet launch ($0.01 < \dot{M}_{\text{out}}/\dot{M}_{\text{acc}} < 0.5$; Cabrit 2009).

For Par-Lup 3-4, \dot{M}_{out} was estimated separately for each lobe, co-adding the spectra over the two regions shown in Figure 2, bottom panels. The [S II] line ratio provides here $n_e = 1150$ and 3200 cm^{-3} , respectively. The [S II] λ 6731 luminosity was evaluated over the same regions, and we take $v_{\text{tan}} = 170 \pm 30 \text{ km s}^{-1}$ in both lobes (Comerón & Fernández 2011). Using Equation (1) we obtain $\dot{M}_{\text{out}} = 3.6 \times 10^{-10} M_{\odot} \text{ yr}^{-1}$ for the blue jet and $3.2 \times 10^{-10} M_{\odot} \text{ yr}^{-1}$ for the red lobe, remarkably similar on the two sides of the system. Therefore, over the two lobes $\dot{M}_{\text{out}}/\dot{M}_{\text{acc}} \sim 0.85$, which is slightly above the maximum indicated for magneto-centrifugal acceleration. The estimated uncertainties on \dot{M}_{acc} and \dot{M}_{out} , however, combined with the partial obscuration of the accretion funnels by the close-to-edge-on disk can lower this value to 0.3–0.5, compatible with that scenario.

Summarizing, X-shooter spectra prove to be fundamental in jet studies as they provide an immediate overview of the outflow kinematics and excitation, as well as rich accretion diagnostics. The first two low-mass (0.5 and $0.13 M_{\odot}$) targets examined proved to have accretion/ejection properties compatible with a magneto-centrifugal scenario. An extension of the current diagnostic techniques to fully exploit the potential of X-shooter spectra is underway and will be presented in a forthcoming paper.

We dedicate this Letter to the memory of Roberto Pallavicini. We thank V. D’Odorico, P. Goldoni, A. Modigliani and the ESO staff for support with the observations and the X-shooter pipeline, and the referee for very useful comments. E. T. Whelan is supported by an IRCSET-Marie Curie Fellowship in Science within the European Community FP7.

REFERENCES

Alcalá, J. M., et al. 2011, *Astron. Nachr.*, **332**, 242
 Bacciotti, F., & Eisloffel, J. 1999, *A&A*, **342**, 717
 Beck, T. L., McGregor, P. J., Takami, M., & Pyo, T.-S. 2008, *ApJ*, **676**, 472

Cabrit, S. 2009, in *Protostellar Jets in Context*, ed. K. Tsinganos, T. Ray, & M. Stute (Astrophysics and Space Science Proceedings Series; Berlin: Springer), 247
 Comerón, F., & Fernández, M. 2011, *A&A*, **528**, 99
 Comerón, F., Fernández, M., Baraffe, I., Neuhauser, R., & Kaas, A. A. 2003, *A&A*, **406**, 1001
 Comerón, F., & Reipurth, B. 2006, *A&A*, **458**, L21
 Comerón, F., Reipurth, B., Henry, A., & Fernández, M. 2004, *A&A*, **417**, 583
 Dame, T. M., et al. 1987, *A&A*, **322**, 706
 Fernández, M., & Comerón, F. 2005, *A&A*, **440**, 1119
 Ferreira, J., Dougados, C., & Cabrit, S. 2006, *A&A*, **453**, 785
 Hartigan, P., Morse, J. A., & Raymond, J. 1994, *ApJ*, **436**, 125
 Hartigan, P., Edwards, S., & Ghandour, L. 1995, *ApJ*, **452**, 736
 Hartigan, P., & Morse, J. 2007, *ApJ*, **660**, 426
 Hartmann, L. 1998, *Cambridge Astrophysics Ser. 32, Accretion Processes in Star Formation* (Cambridge: Cambridge Univ. Press)
 Herczeg, G. J., & Hillenbrand, L. A. 2008, *ApJ*, **681**, 594
 Hirth, G. A., Mundt, R., Solf, J., & Ray, T. P. 1994, *ApJ*, **427**, L99
 Huélamo, N., et al. 2010, *A&A*, **523**, 42
 Kwan, J., Edwards, S., & Fischer, W. 2007, *ApJ*, **657**, 897
 Luhman, K. L. 2007, *ApJS*, **173**, 104
 Masciadri, E., & Raga, A. C. 2004, *ApJ*, **615**, 850
 Melnikov, S. Yu, Eisloffel, J., Bacciotti, F., & Woitas, J. 2009, *A&A*, **506**, 763
 Merín, B., et al. 2008, *ApJS*, **177**, 551
 Modigliani, A., et al. 2010, *Proc. SPIE*, **7737**, 56
 Mohanty, S., Jayawardhana, R., & Basri, G. 2005, *ApJ*, **626**, 498
 Muzerolle, J., Hartmann, L., & Calvet, N. 1998, *AJ*, **116**, 2965
 Nakajima, Y., Tamura, M., Oasa, Y., & Nakajima, T. 2000, *AJ*, **119**, 873
 Natta, A., Testi, L., Muzerolle, J., Randich, S., Comerón, F., & Persi, P. 2004, *A&A*, **424**, 603
 Nisini, B., Bacciotti, F., Giannini, T., Massi, F., Eisloffel, J., Podio, L., & Ray, T. P. 2005, *A&A*, **441**, 159
 Podio, L., Bacciotti, F., Nisini, B., Eisloffel, J., Massi, F., Giannini, T., & Ray, T. P. 2006, *A&A*, **456**, 189
 Podio, L., Eisloffel, J., Melnikov, S., Hodapp, K. W., & Bacciotti, F. 2011, *A&A*, **527**, 13
 Podio, L., Garcia, P. J. V., Bacciotti, F., Antonucci, S., Nisini, B., Dougados, C., & Takami, M. 2008, *A&A*, **480**, 421
 Pudritz, R. E., Ouyed, R., Fendt, C., & Brandenburg, A. 2007, in *Protostars and Planets V*, ed. R. D. Jewitt & K. Keil (Tucson, AZ: Univ. Arizona Press), 277
 Ray, T., Dougados, C., Bacciotti, F., Eisloffel, J., & Chrysostomou, A. 2007, in *Protostars and Planets V*, ed. R. D. Jewitt & K. Keil (Tucson, AZ: Univ. Arizona Press), 231
 Reipurth, B., Pedrosa, A., & Lago, M. T. V. T. 1996, *A&AS*, **120**, 229
 Savage, B. D., & Mathis, J. S. 1979, *ARA&A*, **17**, 73
 Schisano, E., Covino, E., Alcalá, J. M., Esposito, M., Gandolfi, D., & Guenther, E. W. 2009, *A&A*, **501**, 1013
 Shang, H., Li, Z.-Y., & Hirano, N. 2007, in *Protostars and Planets V*, ed. R. D. Jewitt & K. Keil (Tucson, AZ: Univ. Arizona Press), 261
 Takami, M., Chrysostomou, A., Bailey, J., Gledhill, T. M., Tamura, M., & Terada, H. 2002, *ApJ*, **568**, L53
 Whelan, E. T., & Garcia, P. J. V. 2008, in *Jets from Young Stars II: Clues from High Angular Resolution Observations*, ed. F. Bacciotti, E. Whelan, & L. Testi (Lecture Notes in Physics, Vol. 742; Berlin: Springer), 123
 Whelan, E. T., Ray, T. P., Podio, L., Bacciotti, F., & Randich, S. 2009, *ApJ*, **706**, 1054
 Whelan, E. T., et al. 2010, *ApJ*, **720**, L119
 Wichmann, R., Bastian, U., Krautter, J., Jankovics, I., & Rucinski, S. M. 1998, *MNRAS*, **301**, L39